KEK-PREPRINT-92-6
Fermilab Library
0 1190 0015474 4

KEK Preprint 92-6
April 1992
H

Top Physics at Future e^+e^- Colliders Experimental Aspects

Keisuke FUJII

National Laboratory for High Energy Physics(KEK)
Tsukuba, 305, Japan

SMULA
MAY 1 1992

ABSTRACT

Physics opportunities to be opened up by heavy top quark productions at future e^+e^- colliders are explored with an emphasis put on the $t\bar{t}$ pair production process. New features brought out by the large top width are discussed from the experimental point of view. Simulation studies show that various prameters can be determined with a reasonable precision even with rather hard beamstrahlungs.

Plenary talk at the Workshop on Physics and Experiments with Linear Colliders, Saariselka, Finland, Sep.9-14, 1991

National Laboratory for High Energy Physics, 1992

KEK Reports are available from:

Technical Information & Library
National Laboratory for High Energy Physics
1-1 Oho, Tsukuba-shi
Ibaraki-ken, 305
JAPAN

Phone:	0298-64-1171	
Telex:	3652-534	(Domestic)
	(0)3652-534	(International)
Fax:	0298-64-4604	
Cable:	KEKOHO	

Top Physics at Future e^+e^- Colliders
Experimental Aspects

Keisuke FUJII
National Laboratory for High Energy Physics(KEK)
Tsukuba, 305, Japan

ABSTRACT

Physics opportunities to be opened up by heavy top quark productions at future e^+e^- colliders are explored with an emphasis put on the $t\bar{t}$ pair production process. New features brought out by the large top width are discussed from the experimental point of view. Simulation studies show that various fundamental prameters can be determined with a reasonable precision even with rather hard beamstrahlungs.

1. Introduction

The best map we have at present for future explorations of the TeV world is the standard model Lagrangian (L_{SM}) which consists of three sectors. The first is the gauge sector (L_{gauge}) governing the universal gauge forces arising from the gauge symmetry, $SU(3)_C \otimes SU(2)_L \otimes U(1)_Y$. The second is the Higgs sector (L_{Higgs}) representing Higgs force among Higgs scalars responsible for spontaneous symmetry breaking necessary for giving masses to weak bosons. The rest is the Yukawa sector (L_{Yukawa}) describing Yukawa forces which cause the mixing and mass generation of elementary fermions. Although this map is called standard, only a little is known of the Higgs and the Yukawa sectors, reflecting the fact that there are two missing particles, top and Higgs, yet to be discovered. In what follows, we will discuss how to explore these two unknown sectors using top quarks at future e^+e^- linear colliders.

The recent limit on the top quark mass indicates that

$$91 \text{ GeV} < m_t < 200 \text{ GeV}$$

where the lower limit is from a CDF's analysis while the upper limit is from LEP experiments. These limits suggest that the top quark is beyond the LEP-II's reach but guarantee that it is certainly in the future linear colliders' reach. What else do they imply? The heavy top quark opens up several new oppotunities. i) There is a chance to observe top Yukawa interaction. ii) Since the lower limit exceeds the bW threshold, the branching ratio to bW will dominate all the other decay modes. Therefore we can easily identify top quarks using the bW final state. iii) Once the bW threshold is crossed, the top width grows like m_t^3. The top quark we are going to deal with is, thus, not only heavy but also fat(having a large width). The width

is about 1 GeV for m_t = 150 GeV and grows with m_t to as large as 2.5 GeV for m_t = 200 GeV as shown in Fig.1. Because of this large width, we can not expect to do onium spectroscopy as we did for charm and bottom quarks. This seemingly disappointing feature turned out to be advantageous in many ways[1,2,3]. First of all, the large width acts as an infrared cutoff, allowing us very clean tests of QCD. The top decays before forming a t-hadron, thus transfers its spin information to decay daughters. Therefore we can measure the polarization of top quarks, by analyzing angular distributions of the decay products. Yet another point I should make here is the fact that the heavy top decays predominantly into a longitudinal W boson, which is a good probe to investigate the Higgs and the Yukawa sectors through the diagram shown in Fig.2.

The production mechanisms we can exploit to investigate top quark physics are as follows: i)$e^+e^- \to t\bar{t}$, ii) $e^+e^- \to t\bar{t}Z$[4], iii) $e^+e^- \to \nu\bar{\nu}t\bar{t}$[5], and iv) $e^+e^- \to t\bar{t}H$[6]. ii) and iii) are useful to study L_{Higgs} and L_{Yukawa} when the $H \to t\bar{t}$ decay is kinematically allowed, otherwise i) and iv) become very important to measure the top Yukawa coupling. Figs.3-a to -c show the cross sections for these processes as functions of $\sqrt{s}$ for m_t = 100, 150, and 200 GeV. As we can see, the $t\bar{t}$ pair production gives the largest cross section in the energy region of next generation linear colliders. For instance, the expected yield for top pair productions is 5k events/year at $L = 10^{33}\text{cm}^{-2}\text{s}^{-1}$ even in the heaviest case of m_t = 200 GeV. Therefore, in what follows, we will focus our attention to mainly the pair production process.

2. Physics in the $t\bar{t}$ Threshold Region

2.1. Formulation and Physics Involved

Schematically the cross section is calculated as sketched in Fig.4. The first z-dependent factors in the formula correspond to the initial state radiative corrections and the Feynman diagram in the formula represents the full helicity amplitudes including top decays. The QCD and Higgs exchange effects enter the diagram as a vertex correction indicated by Γ. This vertex correction, which is blown up in the same figure, contains essentially all the physics involved in the $t\bar{t}$ threshold studies. Multiple gluon and Higgs exchanges can be treated as a potential in the nonrelativistic approximation justifiable near the threshold[7]. Notice that the top quark propagators in the diagrams contain a finite width which acts as an infrared cutoff. In other words, the top decays in the Coulombic region which means that the topponium system plays the role of a positronium system in QCD. Because of this we can test perturbative QCD without complications introduced by nonperturbative contributions like those from the linear confining potential and hadronizations[3]. Notice also that the heavy top decays before forming a topped meson therefore transferring its polarization information to daughter particles. This enables us to carry out polarization analyses which have been impossible for lighter quark pair productions.

In the top mass range of our interest the width of the resonance Γ_θ is dominated by the single quark decay, so that other decay modes involving $t\bar{t}$ annihilations are negiligible. The $t\bar{t}$ threshold shape thus includes the following parameters:

$$\sigma(\sqrt{s}; m_t, \Gamma_t, \alpha_s(M_Z), M_H, \beta_H)$$

where $\alpha_s(M_Z)$ is the QCD coupling constant, M_H the Higgs mass, and β_H the normalized Yukawa coupling($\beta_H = 1$ for the standard model). Γ_t carries informations on $|V_{tb}|^2$ and new exotic decay modes if any. The most interesting is the Higgs contribution. The Yukawa coupling of the top quark should be very hard to study when $H \to t\bar{t}$ decay is kinematically forbidden. On the other hand, the top quark's Yukawa interaction must be investigated in order to get insight into why the top quark is so heavy compared to other fermions. In the case of light Higgs as expected for SUSY, the studies of $t\bar{t}H$ final states and the $t\bar{t}$ threshold are the only way to do this.

2.2. *Theoretical Expectations*

Using the cross section formula, we examine how the threshold shape changes with the parameters that enter it. The $\alpha_s(M_Z)$ dependence of the threshold shape is shown in Figs.5-a to -c for $m_t = 100, 150$, and 200 GeV. As $\alpha_s(M_Z)$ increases, the QCD potential gets deeper and consequently M_θ shifts downwards. At the same time, since $|R_\theta(0)|^2$ grows, the peak height gets bigger. We can also see how resonances are smeared out by a large Γ_t for a large m_t. Figs.6-a to -c are the same plots for various $|V_{tb}|^2$ values. The resonance width Γ_θ ($\simeq 2\Gamma_t \propto |V_{tb}|^2$) decreases with $|V_{tb}|^2$ and makes the peaks higher while making the tails lower. The most interesting is the Higgs effect. The Higgs effect comes from the Yukawa force given in the first approximation by

$$V_H(r) \simeq -\lambda \frac{e^{-M_H r}}{r} \quad \text{with} \quad \lambda = \frac{\sqrt{2}G_F}{4\pi}(\beta_H m_t)^2$$

representing an attractive force. The smaller the Higgs mass becomes and the bigger β_H and m_t grow, the greater will be the effect of the Yukawa force. Notice that the range of the potential is controlled by M_H and is short compared to the QCD potential. Therefore the Yukawa force does not change the resonance mass very much but makes $|R_\theta(0)|^2$ significantly larger thereby increasing the crossection everywhere. Figs.7-a and -b show how the threshold shape gets modified in the standard model for $m_t = 150$ and 200 GeV, as M_H is changed from 50 GeV to infinity. Figs.8-a and -b, on the other hand, demonstrate the β_H^2 dependence for $M_H = 100$ GeV. $\beta_H^2 = 1$ corresponds to the standard model. The Higgs exchange contributes siginificantly to the cross section in the threshold region.

2.3. *Real Life Experiments*

So far we have been dealing with an ideal case in which neither natural beam energy spread nor beamstrahlung modify the threshold shape. Here we take these complications into account and look at how they deform the threshold shape. From now on we restrict ourselves to the $m_t = 150$ GeV case. Fig.9-a shows the effective center of mass energy distribution in the presence of beam energy spread and beamstrahlung. The sharp peak at $\sqrt{s_{eff}}/\sqrt{s_0} = 1$(the δ-function part) corresponds to the no beamstrahlung case, while the long tail downwards represents the effect of beamstrahlung. When we convolute this with the theoretical expectation we discussed in the previous section, we obtain Fig.9-b. One should notice that the peak smearing is mostly due to the beam energy spread, while the effect of the beamstrahlung is essentially a loss of usable luminosity. In order to see this more clearly, let us switch off the beamstrahlung and see how the beam energy spread smears out the resonance peak. Fig.10-a plots the reduced center of mass energy distribtuions for various beam energy widths, where two kinds of spectra, flat-top and double-peak which is more realistic, are compared. The corresponding threshold shapes are shown in Fig.10-b. We can see that as the beam energy spread increases, the first resonance peak quickly disappears.

We should also be aware of the dependence on the structure inside the δ-function part. For detailed studies of the threshold shape, we need to know the beam energy spectrum with a high energy resolution. MILLER proposed a method to measure this effective center of mass energy spectrum[8]. His method consists of two steps. In the first step, we measure undistorted beam energies of electrons and positrons separately. The experience at SLC suggests that the precision obtainable at this stage is 1/2500. In the second step, we look at Bhabha events and measure acollinearity. Using the undistorted beam energy distributions and the acollinearity angle distribution, we estimate the effective center of mass energy distribution. According to his calculations, a precision better than 1/1000 can be expected.

Monte Carlo Event Generation

Before moving on to event selection, it is useful to make a few comments on the Monte Carlo event generation. When the top width exceeds a typical hadronization scale, there will be no t-hadron formation[1,2,9]. Then the polarization information of parent top quarks is transfered to decay daughters which give rise to angular correlations in the final state particles. In order to take proper account of this effect, we should use the full helicity amplitudes. As for the color neutralization, we assume that the color flux is spanned between b and $\bar{b}$ quarks. Since we are going to reconstruct top quarks by jet invariant mass method, it is also important to consider gluon emissions from b or $\bar{b}$ quarks as well as those from W decay daughters. The point here is the energy scale to be used for the parton showering from b or $\bar{b}$ quarks. We should not, for instance, set $Q_{max} = \sqrt{(p_b + p_{\bar{b}})^2}$, but, instead, should set $Q_{max} = m_t - M_W$, since the gluon emission is controlled by the acceleration the b or $\bar{b}$ quarks receive

when their parent t or $\bar{t}$ quarks decay[10]. Consequently, the 4-momentum adjustments after parton showering should be made within the bW systems. The gluon emissions from t or $\bar{t}$ quarks, which are not inculded here could modify the event shape. We assume, however, that there will be no soft-gluons from t or $\bar{t}$ quarks, again because of the large top width acting as an infrared cutoff. Therefore its effect on the event selection efficiency we are going to discuss in the following section will be $O(\alpha_s)$. It is also essential to include initial state radiations as well as beam energy spread and beamstrahlung, since they may change the event shape significantly.

Event Selection

The signature of $t\bar{t}$ pair production is two b quarks and two W bosons in the final state. The two W bosons decay into either $q\bar{q}'$ or $l\bar{\nu}$. Therefore the final state configurations are i) two b-jets and four jets from W's(45 %), ii) two b-jets, two jets and one charged lepton(44 %), and iii) two b-jets and two charged leptons(11 %). There are a lot of contributions made at this conference on $t\bar{t}$ event selection. VENTURI, et al. studied i) and ii), PETRAZA studied ii), and FUJII studied i). There is also a study concerning iii) by IGO-KEMENES. The usefulness of b-tagging was demonstrated by VENTURI, et al. We are not getting into details of the event selections but just mention that the basic cuts used in these analyses can be classified into the following three groups: a) event shape cuts such as those on the number of charged particles, the number of jets, and thrust, b) mass cuts to select W's and t's by jet invariant mass method, and c) requirements of leptons in cases ii) or iii).

In order to measure the threshold shape reliably, we need to select $t\bar{t}$ events with a good S/N ratio. In the case of JLC parameters, the effective cross section at the threshold is about 0.4 pb for $m_t = 150$ GeV while that of the largest background(W^+W^- productions) is about 14 pb. We need some 10^{-3} suppression. Let us see how this can be achieved, taking case i) as an example. Fig.11-a shows a typical 6-jet event expected for case i). When we look at this event in the calorimeter, we have Fig.11-b where we can clearly see six jets. Histogrammed in Figs.12-a and -b are the visible energy and the transverse momentum for the intial sample, respectively, where the final sample distributions are also shown as hatched histograms. Fig.13 is the scatter plot of the 2-jet invariant masses corresponding to two W candidates for the final sample where their projections are also shown. The cut on the invariant masses is depicted as a square in the figure. Fig.14 is a similar plot for the 3-jet invariant masses corresponding to the bW candidates at the threshold. The smooth curve indicates the location of the m_t cut. Finally, Fig.15 shows the thrust distributions for the $t\bar{t}$ signals and the W^+W^- background, just before the final thrust cut indicated by an arrow in the same plot. After this final cut, the detection efficiency is 26 % while the signal to background ratio greater than 10. This detection efficiency translates to about 58 % when the $W \to q\bar{q}$ branching ratio of 67 % is taken into account. We can obtain similar efficiencies and signal to background ratios for cases ii) and iii).

Determination of Various Parameters

Using the $t\bar{t}$ sample so obtained, we can determine the parameters that enter

the threshold formula. The question is how well we can do this. KOMAMIYA[11] made the first attempt to answer it, assuming no beam energy spread and beamstrahlung. Then FUJII[12] studied the same problem with beam energy spread and beamstrahlung taken into account. At this conference, MIQUEL compared various machine parameters and FUJII refined the analysis using a new formalism[13] to calculate the threshold cross section.

Fig.16-a is an example of the energy scan to determine m_t and $\alpha_s(M_Z)$. Each data point corresponds to 1 fb^{-1} and was generated with $|V_{tb}|^2 = 1$, $\alpha_s(M_Z) = 0.12$, and $M_H = \infty$(no Higgs). By fitting these data points to the threshold formula convoluted with the natural beam energy spread and the beamstrahlung spectra, we obtain a contour plot shown in Fig.16-b. The strong correlation between m_t and $\alpha_s(M_Z)$ stems from the fact that the resonance mass decreases as $\alpha_s(M_Z)$ increases. If $\alpha_s(M_Z)$ is known, we have $\Delta m_t \simeq 0.1$ GeV and even if $\alpha_s(M_Z)$ is totally unconstrained, we can expect $\Delta m_t \simeq 0.3$ GeV. Fig.17-a is a similar plot for the determination of $|V_{tb}|^2$. Again we assume 1 fb^{-1} per point. The corresponding contour plot(Fig.17-b) shows no correlation between m_t and $|V_{tb}|^2$ and indicates $\Delta|V_{tb}|^2 \simeq 0.15 \sim 0.20$. Figs.18-a and -b are examples for the M_H and β_H measurements where the energy points are chosen in the same way as with Figs.16-a and 17-a. The M_H-β_H^2 contour is given in Fig.18-c. In the case of $\beta_H^2 = 1$(SM) the scan is sensitive to a M_H up to about 120 GeV. It should be noted that the energy points used here are by no means optimized. Prior to the actual energy scan, we will have a fairly good estimate of m_t as described in the next section. Based on this knowledge, we should be able to improve the precision of the measurements by optimizing the energy points to maximize the sensitivities to the model parameters discussed above.

3. Physics in the Open Top Region

The physics we can extract from the $t\bar{t}$ productions in the region well above the threshold is essentially the same as that in the threshold region. The loop corrections to the $t\bar{t}\gamma$ and $t\bar{t}Z$ vertices involve M_H, β_H, and $\alpha_s(M_Z)$ as discussed by KÜHN at this conference. In addition, we can perform detailed studies of top decays taking advantage of the large cross seciton. Here we discuss three methods to determine m_t[14] and the polarization measurement of t quarks and that of W bosons originating from them[12,15].

3.1. *Determination of m_t*

Hemisphere Mass Method

The first method is to look at the heavier hemisphere mass when an event is divided into two hemispheres by the plane perpendicular to the sphericity axis. The resultant hemisphere mass is shown in Fig.19 for $m_t = 120$ GeV and $\sqrt{s} = 500$ GeV where the distributions for generated and reconstructed events are compared. We can see a clear top mass peak. The long tail on the lower mass side is due to missing neutrinos. Apparently, this method relies on a good hemisphere separation that means a sufficient boost. The expected statistical error on m_t is 0.2 GeV for $m_t = 120$ GeV which gradually degradates to 0.4 GeV for $m_t = 150$ GeV, when we accumulate ~ 7 fb^{-1}. The method seems to work for $m_t < 0.6E_{beam}$.

3-Jet Mass Method

We can also try to determine m_t from the jet invariant mass by reconstructing the three jets from the top quark decay. Fig.20 is an example of the 3-jet invariant mass for $m_t = 150$ GeV and $\sqrt{s} = 500$ GeV. The distribution peaks at $m_t = 150$ GeV over a broad background coming from wrong combinations. The mass peak has a width of about 3.3 GeV which implies a statistical accuracy on the peak position of 0.1 GeV for 1000 detected t quarks corresponding to 10 fb^{-1}. This method seems to work in the wide energy range: $m_t < 0.9E_{beam}$.

End Point Method

The end points of the momentum spectrum of W's from t decays carry information of m_t through the following relations:

$$E_W^* = \frac{m_t^2 + M_W^2}{2m_t}$$

$$\beta_W^* = \frac{m_t^2 - M_W^2}{m_t^2 + M_W^2}$$

$$E_W = \gamma_t E_W^*(1 + \beta_t \beta_W^* \cos\theta^*)$$

where the last equation determines E_W^{min} and E_W^{max} which in turn fix p_W^{min} and p_W^{max} as functions of m_t. By selecting events where one W decays into $q\bar{q}$ and the other into $l\bar{\nu}$, we can measure the momentum of the W which decayed leptonically as

$$p_W = (\sqrt{s}, 0) - \sum_{i \neq l} p_i.$$

Events badly distorted by initial state radiation or beamstrahlung can be eliminated by applying a cut on p_W^2. Fig.21 shows the distribution of so reconstructed p_W for

$m_t = 140$ GeV at $\sqrt{s} = 282$ GeV. The expected statistical error on p_W end points is about 2 GeV which translates to 0.4 GeV on m_t for 12 fb^{-1}($\sim$ 400 events). The method has the largest sensitivity in the threshold region and can be used to cross-check the m_t measurement by the threshold scan.

The quoted errors were, of course, all purely statistical. In practice we have to take into account various systematic errors introduced through imperfect calorimeter calibration and uncertainties in QCD corrections including hadronization. The QCD corrections could happen to be small due to the infrared cutoff introduced by large top width. Here we need theorists' help.

3.2. *Measurement of W Polarization*

As shown in Fig.1, the heavy top quark decays predominantly to a longitudinally polarized W boson(W_L). Since the W_L originates from the spontaneous symmetry breaking, the top quark decay provides a powerful handle to investigate L_{Higgs} and L_{Yukawa}. As a matter of fact, even within the framework of the standard model, there exists a diagram(see Fig.2) which contains both ttH and WWH couplings which should modify the branching fraction to the transverse(W_T) and the longitudinal W bosons. Since theoretical calculations are not yet completed, here we focus our attention on how well we can measure the branching fraction R defined by

$$R = \frac{\Gamma(t \to bW_L)}{\Gamma(t \to bW_T) + \Gamma(t \to bW_L)}.$$

The polarization state of the W boson can be determined by observing the angular distribution of $W \to q\bar{q}'$ decays in the W's helicity frame. The angular distribution is given by

$$\frac{dN}{d\cos\theta} = \frac{3}{4}N_L(1 - \cos^2\theta) + \frac{3}{8}N_T(1 + \cos^2\theta)$$

where N_T and N_L stand for the numbers of the top quarks decaying into W_T and W_L, respectively. By fitting this formula to the observed angular distribution, we can determine N_T and N_L and consequently the branching fraction:

$$R = \frac{N_L}{N_T + N_L}.$$

Fig.22 is an example of the helicity angle distribution for jets from W decays. We can see that the Monte Carlo data points agree well with the standard model prediction shown as a solid line. The R value and its expected error are plotted as functions of m_t in Fig.23 where the 1-σ bound corresponds to 1k top decays. A data sample of 10 fb^{-1} at $\sqrt{s} = 350$ GeV enables us to determine the branching fraction with a precision of

$$\frac{\sigma_R}{R} \simeq 0.017 \text{ (stat. only)}$$

which is very encouraging.

3.3. *Measurement of t Polarization*

The power of the anglular analysis is more prominent when we consider anomalous couplings at the tbW vertex. SCHUMIDT[16] carried out systematic theoretical studies on the effects of anomalous couplings by parametrizing them as:

$$tbW \text{ vertex} = F_{1L}\gamma^{\mu}P_L + \frac{i\sigma^{\mu\nu}}{2m_t}q_\nu F_{2L}P_R + F_{1R}\gamma^{\mu}P_R + \frac{i\sigma^{\mu\nu}}{2m_t}q_\nu F_{2R}P_L$$

where the standard model corresponds to $F_{1L} = 1$ and all the others zero. PETRAZA[15] made a simulation study to see how sensitive the angluar analysis is to these anomalous couplings. The analysis goes as follows. First, we cut the cosine of the top quark's production angle and select the forward scattering events. When the incoming electron beam is polarized, this cut effectively selects a particular helicity combination of the $t\bar{t}$ system. Then we look at the decay angles: $\cos\chi_W$ and $\cos\chi_l$ where χ_W is the helicity angle of W in the t rest frame and χ_l is that of the lepton in the W rest frame. Fig.24-a is a lego plot of these two angles for $F_{1L} = 0$ and $F_{1R} = 1$ which should be compared with Fig.24-b for the standard model case: $F_{1L} = 1$ and $F_{1R} = 0$. The Monte Carlo data correspond to 10 fb^{-1} with an electron beam polarization of 80 %. The difference is clear. The expected sensitivity to the anomalous couplings is about 10 %.

4. High Energy Processes

At higher energies, we can use other processes to invistigate L_{Higgs} and L_{Yukawa} as seen in Fig.3. In particular, if $H \to t\bar{t}$ is kinematically allowed, we can study top Yukawa interaction directly by studying this decay mode. If it is not, we have to rely on either the $t\bar{t}$ threshold study as described above or the measurement of $t\bar{t}H$ final state. The latter process was discussed by DJOUADI[6] at this conference. Although the result of his study seems promising, we should wait for detailed Monte Carlo studies before drawing definite conclusion. Here we shall examine $e^+e^- \to t\bar{t}Z$ and $e^+e^- \to \nu\bar{\nu}t\bar{t}$ processes, for which Monte Carlo simulation studies have been made.

4.1. $e^+e^- \to t\bar{t}Z$

Fig.25 shows the total cross sections at $\sqrt{s} = 0.6$ and 1.0 TeV for $e^+e^- \to t\bar{t}Z$ as functions of Higgs mass, where top mass is assumed to be 130 GeV. We can see that the contribution from virtual Higgs is very small[17]. Therefore, the determination of top Yukawa coupling is possible, only when $H \to t\bar{t}$ decay mode is open. TAUCHI et al.[4] studied such a case. They selected 8-jet events and reconstructed $t\bar{t}Z$ final states. Plotted in Fig.26 is the invariant mass distribution for the $t\bar{t}$ system. We can see a Higgs mass peak over a broad background from non-Higgs diagrams. Backgrounds

from other processes are negligible. The detection efficiency including the branching ratio to 8-jet final states is about 20 %. The expected precision for top Yukawa coupling is $\sigma_{\beta_H}/\beta_H \simeq 0.1$ for an integrated luminosity of 60 fb^{-1}.

4.2. $e^+e^- \to \nu\bar{\nu}t\bar{t}$

Unlike the $t\bar{t}Z$ case, the virtual Higgs effect is sizable for $e^+e^- \to \nu\bar{\nu}t\bar{t}$, as seen from Fig.27(notice that cross sections are plotted in logarithmic scale here). Therefore this process might allow us to measure top Yukawa coupling, even if $H \to t\bar{t}$ is kinematically forbidden. This requires, however, a very high luminosity. TSUKAMOTO[5] assumed more realistic luminosity and studied the case where the $t\bar{t}$ decay mode is open. He required 6-jet topology and looked at the invariant mass for the $t\bar{t}$ system which is shown in Fig.28-c where $m_t = 150$ GeV, $M_H = 600$ GeV, and $\sqrt{s} = 1$ TeV. Figs.28-a, -b and -d are those for the following background processes: a) $t\bar{t}Z$, b) $t\bar{t}$, and d) $e^+e^-t\bar{t}$. The overall detection efficiency including the branching ratio is 12 % for the signal events. The assumed integrated luminosity is 300 fb^{-1} corresponding to 96 signal events which should be compared with 143 events from the three background processes. The expected statistical error on top Yukawa coupling is $\sigma_{\beta_H}/\beta_H \simeq 0.08$. It should be emphasized that the cross section for signal events becoms about four times larger at $\sqrt{s} = 1.5$ TeV, while that for the major background($t\bar{t}$) decreases by about a factor of two. The advantage of a higher energy machine is obvious for this process.

Though not studied yet, there is one important possibility to improve the accuracy of the measurement of top Yukawa coupling. That is to project out spin-0 component. This possibility should be investigated in future simulation studies.

5. Conclusions

In order to demonstrate physics oppotunities to be opened up by heavy top quark productions, simulation studies were carried out for the following three processes: i) $e^+e^- \to t\bar{t}$, ii) $e^+e^- \to t\bar{t}Z$, and iii) $e^+e^- \to \nu\bar{\nu}t\bar{t}$.

Most of the simulation studies presented at this conference were focused on the first process, which has the largest cross section in the energy region of next generation linear colliders. From the experimental point of view, this process involves all the essential features of analysis procedure necessary for top quark studies. First of all, the event selection scheme based on parton reconstruction by jet invariant method can be applied to any process with top quarks in final states. It was shown that the identification of top quark is relatively easy: we can achieve an overall detection efficiency of 10 to 30 % with a signal to background ratio of 3 to 10. Here we should emphasize that these numbers will not change very much, even if there are some exotic decay modes such as $t \to bH^+$ or $t \to \tilde{t}\tilde{Z}$, since the $t \to bW^+$ mode is always expected to dominate the others.

The selected $t\bar{t}$ sample can be used to determine various parameters. A threshold scan consisting of 11 energy points each with an integrated luminosity of 1 fb^{-1}, for instance, can determine m_t with a precision of about 0.3 GeV for a top quark with a mass of about 150 GeV, even if we do not know α_s at all. If α_s is known, the precision will improve to 0.1 GeV. Conversely, if m_t is given, we can measure α_s with $\Delta\alpha_s \simeq 0.002$. Notice that this α_s measurement is largely free from complications due to non-perturbative QCD effects. The threshold scan also allows us to determine the top width with a precision of about 20 %. More interesting is the possibility to observe the effect of Higgs exchange. For the standard model Higgs, the sensitivity to this effect extends up to $M_H \simeq 120$ GeV. In order to investigate Yukawa interactions of a top quark heavier than $M_H/2$, the threshold scan will provide us with invaluable information together with the analysis of the $e^+e^- \to t\bar{t}H$ process. All of these results assume that the differential luminosity is known precisely. A method is proposed at this conference to measre it. Its validity should be examined in detail in future studies.

In the open top region, there are other possibilities for m_t measurements. At this conference, three such possibilities were studied: a) hemispher mass method, b) 3-jet mass method, and c) end point method. All of these methods are promising and will determine m_t to a statistical accuracy of less than 0.5 GeV for a 150 GeV top, with an integrated luminosity of 10 fb^{-1}. The analysis of theoretical error concerning the QCD corrections including hadronization is very important here.

Another important feature of heavy top physics is the possibility of decay angle measurements. For instance, the 3-jet mode can be used to study the branching fraction of $t \to bW_L$ which should be sensitive to both the Higgs and the Yukawa couplings. The angular analysis of the W decays allows us to determine the branching fraction to W_L with a statistical error of $\Delta R/R \simeq 0.017$. We can also measure the helicity angle of the b quark in the t rest frame simultaneously with that of a lepton from the W decay in the W rest frame. Such a full angular analysis enables us to investigate the tbW vertex in detail. For instance, a 10 % measurement of anomalous coupling seems quite feasible.

At even higher energies, we can use processes ii) and iii) to determine top Yukawa coupling, which will be very useful, in particular, when $H \to t\bar{t}$ decay is kinematically allowed. The expected precision on top Yukawa coupling is about 10 % for process ii), when we assume $M_H = 300$ GeV, $m_t = 130$ GeV, and an integrated luminosity of 60 fb^{-1} at $\sqrt{s} = 600$ GeV. Process iii), on the other hand, allows us an 8 % measurement of top Yukawa coupling for $M_H = 600$ GeV and $m_t = 150$ GeV, if an integrated luminosity of 300 fb^{-1} is accumulated at $\sqrt{s} = 1$ TeV.

In conclusion, we have studied the top quark physics at next generation linear colliders in the light of the standard model Lagrangian. However, if the Higgs sector is weakly coupled and if SUSY is the scenario for us, there are a lot of possibilities of new particles such as charged Higgs and super particles appearing in the top decay. We should investigate these possibilities not to mention the more practical problems like

how to measure luminosity with a precision which matches the physics requirements or how to optimize the machine parameters for the $t\bar{t}$ studies, etc.

Acknowledgements:

The author wishes to thank all the members of the JLC physics working group for useful discussions and comments. In particular, K. Hagiwara, K. Hikasa, Y. Sumino, C. Ng, and H. Murayama deserve special mention. If it were not for their contributions, this work could not be completed. The author is very grateful to Professors W. de Boer, V. Khoze, J. Kühn, M. Peskin, and P. Zerwas for valuable discussions. He also thanks Prof. P. Igo-kemenes and M. Petraza for providing their results and giving fruitful suggestions. Finally, the author would like to express his heartfelt gratitude to the conference organizers for their painstaking efforts to make this conference so comfortable and so successful.

REFERENCES

1. J. Kühn, *Acta Physica Austriaca, Suppl.* **XXIV** (1982) 203.
2. I. Bigi, Y. Dokshitzer, V. Khoze, J. Kühn, and P. Zerwas, *Phys. Lett.*, **B181** (1986) 157.
3. V. Fadin and V. Khoze, *Sov. J. Nucl. Phys.* **48** (1988) 309, M. Strassler and M. Peskin, *Phys. Rev.* **D43** (1991) 1500.
4. T. Tauchi, K. Fujii, and A. Miyamoto, KEK Preprint 90-148 (1990).
5. T. Tsukamoto, KEK Preprint 91-17 (1991).
6. A. Djouadi, talk given at this conference. A. Djouadi, J. Kalinowski, and P. Zerwas, DESY 91-104.
7. K. Hagiwara, K. Kato, A. Martin, and C. Ng, *Nucl. Phys.* **B344** (1990) 1.
8. D. Miller, talk given at this conference.
9. L. Orr and J. Rosner, *Phys. Lett.* **B246** (1990) 221.
10. K. Hagiwara, private communication.
11. S. Komamiya, SLAC-PUB-5324 (1991).
12. K. Fujii, KEK Preprint 90-187 (1991).
13. Y. Sumino, K. Fujii, K. Hagiwara, H. Murayama, and C. Ng, in preparation.
14. W. de Boer, talk given at this conference.
15. M. Petraza, talk given at this conference.
16. C. Schumidt, talk given at this conference.
17. K. Hagiwara, H. Murayama, and I. Watanabe, KEK Preprint 90-125 (1990).

FIGURE CAPTIONS

1) Top quark width as a function of top mass.

2) A 1-loop diagram in the standard model which contains both the Higgs and the Yukawa couplings.

3) Total cross sections for $t\bar{t}$, $t\bar{t}Z$, $\nu\bar{\nu}t\bar{t}$, and $t\bar{t}H$ productions for three representative top masses: (a) $m_t = 100$ GeV, (b) $m_t = 150$ GeV, and (c) $m_t = 200$ GeV.

4) A schematic diagram for cross section evaluation.

5) Threshold shape for various $\alpha_s(M_Z)$ values: (a) $m_t = 100$ GeV, (b) $m_t = 150$ GeV, and (c) $m_t = 200$ GeV.

6) Threshold shape for various $|V_{tb}|^2$ values, where $|V_{tb}|^2$ is defined to be $\Gamma_t/\Gamma_t(\mathrm{SM}; |V_{tb}|^2 = 1)$: (a) $m_t = 100$ GeV, (b) $m_t = 150$ GeV, and (c) $m_t = 200$ GeV.

7) Threshold shape for various M_H for the standard model Higgs: (a) $m_t = 150$ GeV and (b) $m_t = 200$ GeV.

8) Threshold shape for various β_H^2 for $M_H = 100$ GeV, where β_H is the normalized top Yukawa coupling($\beta_H = 1$ in the standard model): (a) $m_t = 150$ GeV and (b) $m_t = 200$ GeV.

9) (a) The effective center of mass energy distribution in the presence of beam energy spread and beamstrahlung. (b) Threshold shapes before and after the inculsion of the natural beam energy spread and beamstrahlung.

10) (a) The reduced center of mass energy distributions including the effects of initial state radiations and natural beam energy spread but leaving out the effect of beamstrahlung. Distributions for two kinds of spectra, flat-top and double-peaked which is more realistic, are shown for various beam energy spreads. (b) Corresponding threshold shapes.

11) (a) A typical 6-jet event from $e^+e^- \to t\bar{t} \to bW^+\bar{b}W^-$ where both W^+ and W^- decay into $q\bar{q}$. (b) The same event in the calorimeter.

12) (a) E_{vis} and (b) P_T distrigutions for intial(open histograms) and final(hatched histograms) samples.

13) A scatter plot of the invariant masses of the 2-jet systems reconstructed as W boson candidates together with their projection to each axis.

14) A similar plot for the invariant masses of the 3-jet systems reconstructed as bW candidates at the $t\bar{t}$ threshold.

15) Thrust distributions for the $t\bar{t}$ signal and the W^+W^- background with all but the thrust cut indicated by an arrow.

16) (a) An example of energy scan to determine m_t and $\alpha_s(M_Z)$ where each point corresponds to 1 fb^{-1}. (b) The contour resulting from the fit to the data points.

17) (a) An example of energy scan to determine m_t and $|V_{tb}|^2$ where each point corresponds to 1 fb^{-1}. (b) The contour resulting from the fit to the data points.

18) (a) An example of energy scan to determine M_H and β_H^2 where the effective cross section curves are superimposed for several M_H values. (b) The same plot with the effective cross section curves for several β_H^2 values. (c) The contour resulting from the fit to the data points.

19) Heavier hemispher mass distributions for $m_t = 120$ GeV and $\sqrt{s} = 500$ GeV. The open histogram is the distribution of generated events while the hatched histogram is that of reconstructed events.

20) Invariant mass distribution for the 3-jet system resulting from $t \to bW$ decays.

21) The momentum distribution of Ws from t decays for $m_t = 120$ GeV and $\sqrt{s} = 282$ GeV.

22) Helicity angle of q or $\bar{q}$ from W decay.

23) Branching fraction of the $t \to bW_L$ decay as a function of m_t. The dashed curves indicate 1-σ boundaries expected for 1k top decays.

24) The top decay angle distributions for (a) $F_{1L} = 0$ and $F_{1R} = 1$ and (b) $F_{1L} = 1$ and $F_{1R} = 0$(Standard Model). χ_W is the helicity angle of W in the t rest frame and χ_l is the helicity angle of the lepton in the W rest frame.

25) The cross sections for $e^+e^- \to t\bar{t}Z$ at $\sqrt{s} = 0.6$(solid line) and 1.0 TeV(dashed line) for $m_t = 130$ GeV as functions of Higgs mass. For comparison, the cross sections for no Higgs case are also shown.

26) The invariant mass of the $t\bar{t}$ system for the process $e^+e^- \to t\bar{t}Z$, where $m_t = 130$ GeV, $M_H = 300$ GeV, and $\sqrt{s} = 0.6$ TeV. Data points are Monte Carlo result corresponding to 60 fb^{-1}. The solid histogram is the background from non-Higgs diagrams, while the dashed includes the contribution from Higgs decays.

27) The cross sections for $e^+e^- \to \nu\bar{\nu}t\bar{t}$ at $\sqrt{s} = 1.0$(solid line) and 1.5 TeV(dashed line) for $m_t = 150$ GeV as functions of Higgs mass. The cross sections for no Higgs case are also plotted to see the virtual Higgs contribution.

28) The invariant mass distributions for the $t\bar{t}$ system for (a) $e^+e^- \to t\bar{t}Z$, (b) $e^+e^- \to t\bar{t}$, (c) $e^+e^- \to \nu\bar{\nu}t\bar{t}$, and (d) $e^+e^- \to e^+e^-t\bar{t}$, where $m_t = 150$ GeV, $M_H = 600$ GeV, and $\sqrt{s} = 1.0$ TeV are assumed. The number of events corresponds to an integrated luminosity of 300 fb^{-1}.

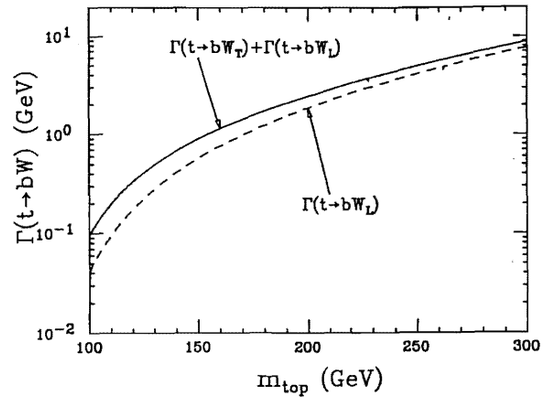

Fig.1 Top quark width as a function of top mass.

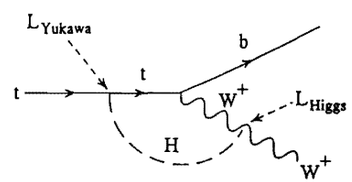

Fig.2 A 1-loop diagram in the standard model which contains both the Higgs and the Yukawa couplings.

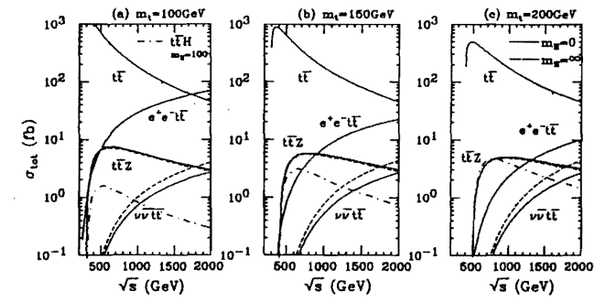

Fig.3 Total cross sections for $t\bar{t}$, $t\bar{t}Z$, $\nu\bar{\nu}t\bar{t}$, and $t\bar{t}H$ productions for three representative top masses: (a) $m_t = 100$ GeV, (b) $m_t = 150$ GeV, and (c) $m_t = 200$ GeV.

$$\sigma = \left(1+\frac{2\alpha}{\pi}\left(\frac{\pi^2}{6}-\frac{1}{4}\right)\right)\int_0^1 dz\,\beta_e\left(z^{\beta_e-1}\left(1+\frac{3}{4}\beta_e\right)-\left(1-\frac{1}{2}z\right)\right)$$

$$\beta_e = \frac{2\alpha}{\pi}\left(\ln\left(\frac{s}{m_e^2}\right)-1\right)$$

$$\hat{s} = (1-z)s$$

where

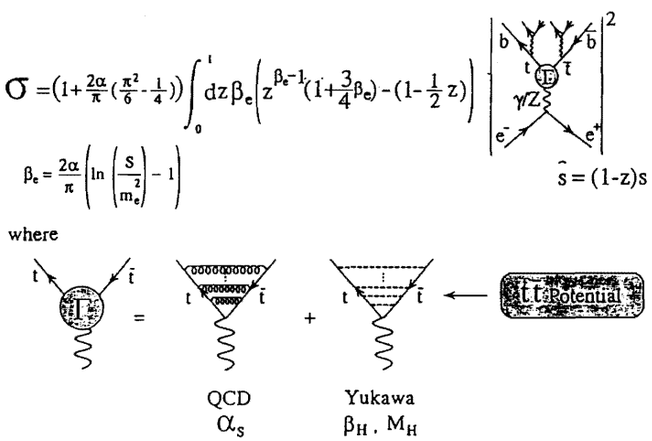

Fig.4 A schematic diagram for cross section evaluation.

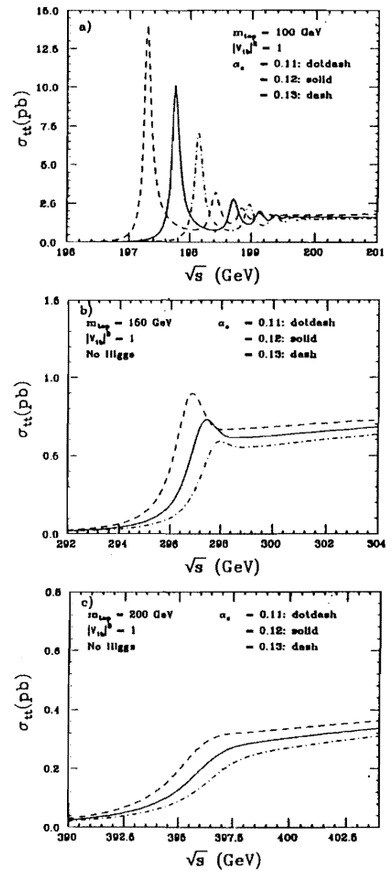

Fig.5 Threshold shape for various $\alpha_s(M_Z)$ values: (a) m_t = 100 GeV, (b) m_t = 150 GeV, and (c) m_t = 200 GeV.

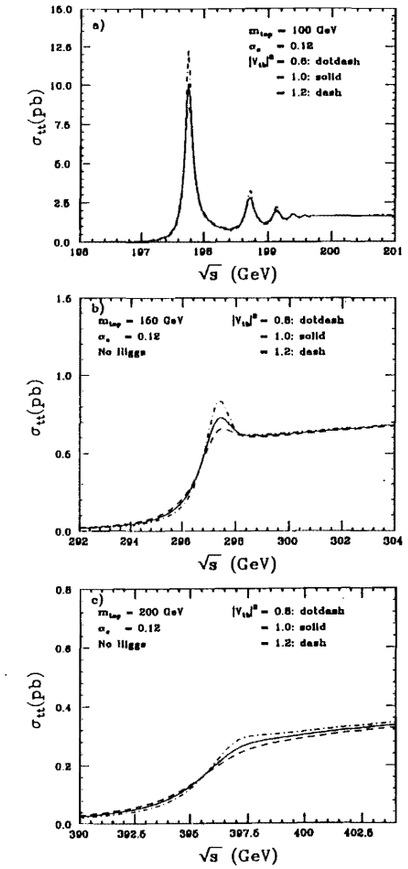

Fig.6 Threshold shape for various $|V_{tb}|^2$ values, where $|V_{tb}|^2$ is defined to be $\Gamma_t/\Gamma_t(\mathrm{SM};|V_{tb}|^2 = 1)$: (a) m_t = 100 GeV, (b) m_t = 150 GeV, and (c) m_t = 200 GeV.

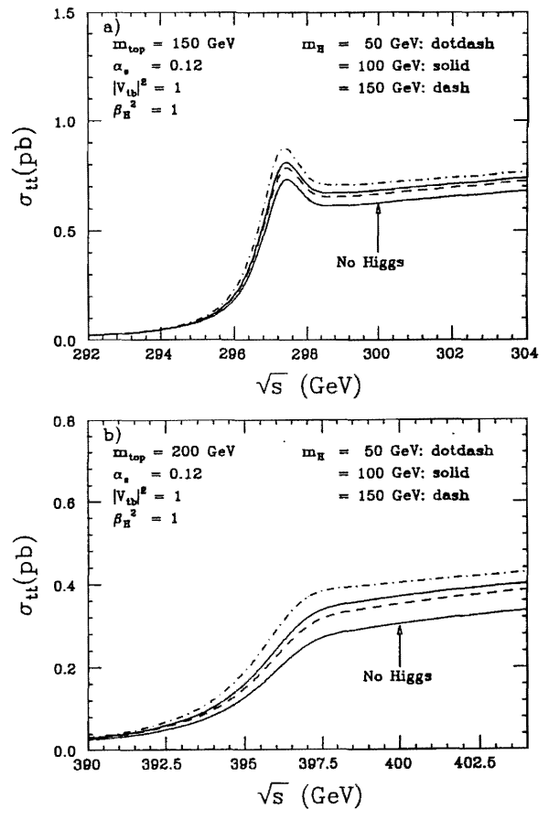

Fig.7 Threshold shape for various M_H for the standard model Higgs: (a) m_t = 150 GeV and (b) m_t = 200 GeV.

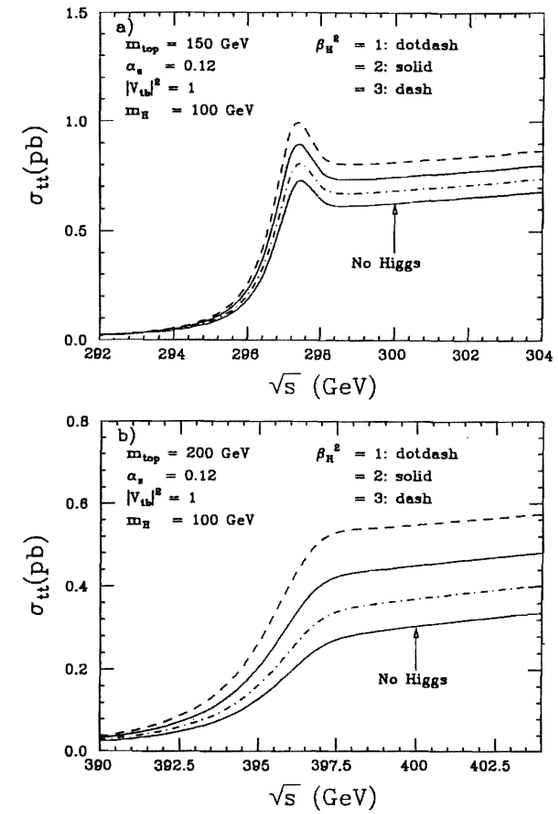

Fig.8 Threshold shape for various β_H^2 for M_H = 100 GeV, where β_H is the normalized top Yukawa coupling(β_H = 1 in the standard model): (a) m_t = 150 GeV and (b) m_t = 200 GeV.

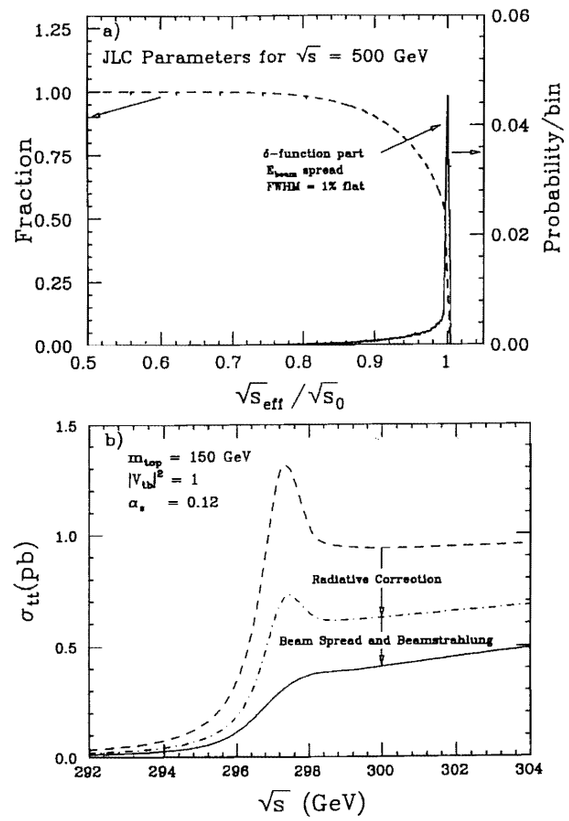

Fig.9 (a) The effective center of mass energy distribution in the presence of beam energy spread and beamstrahlung. (b) Threshold shapes before and after the inculsion of the natural beam energy spread and beamstrahlung.

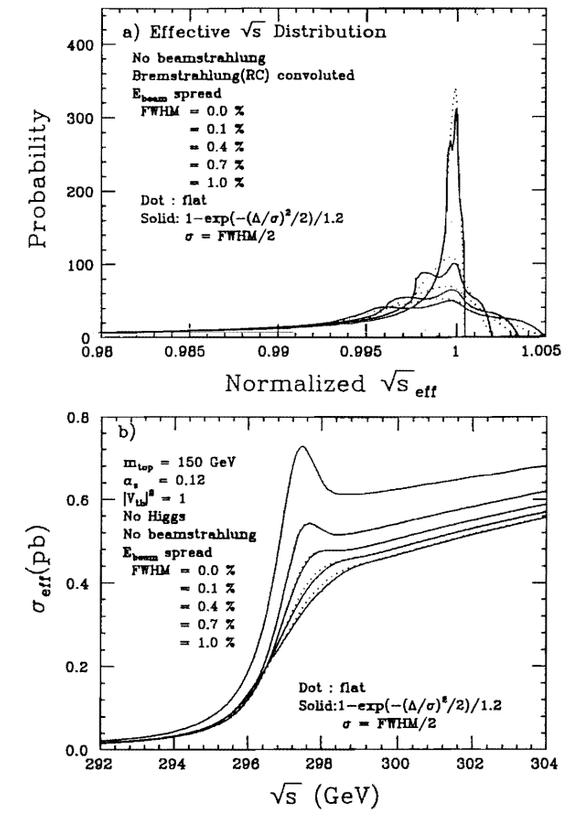

Fig.10 (a) The reduced center of mass energy distributions including the effects of initial state radiations and natural beam energy spread but leaving out the effect of beamstrahlung. Distributions for two kinds of spectra, flat-top and double-peaked which is more realistic, are shown for various beam energy spreads. (b) Corresponding threshold shapes.

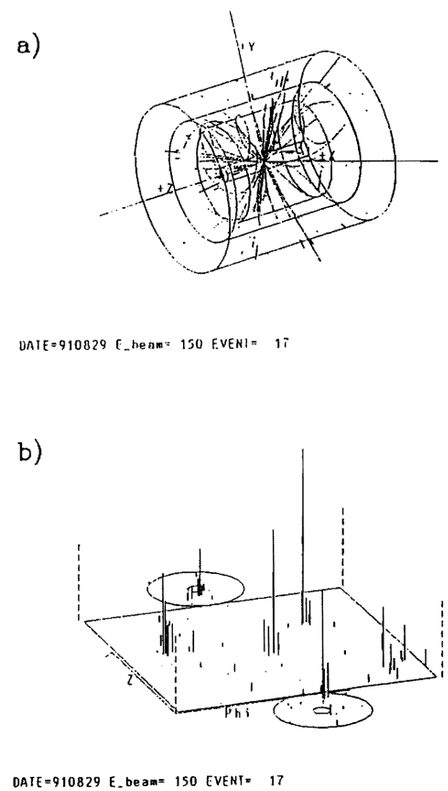

Fig.11 (a) A typical 6-jet event from $e^+e^- \to t\bar{t} \to bW^+\bar{b}W^-$ where both W^+ and W^- decay into $q\bar{q}$. (b) The same event in the calorimeter.

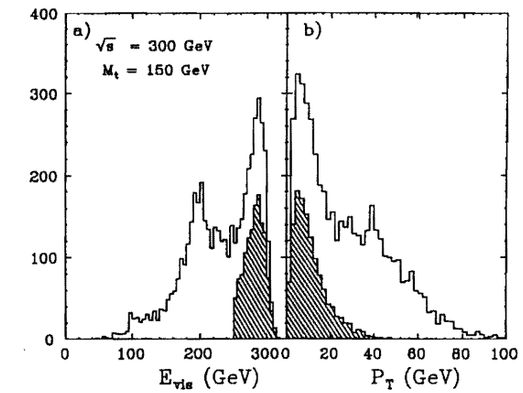

Fig.12 (a) E_{vis} and (b) P_T distrigutions for intial(open histograms) and final(hatched histograms)

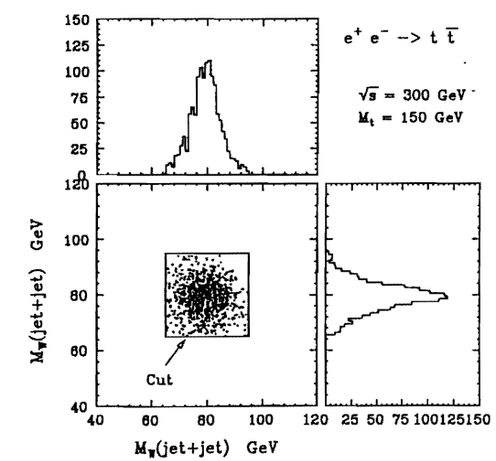

Fig.13 A scatter plot of the invariant masses of the 2-jet systems reconstructed as W boson candidates together with their projection to each axis.

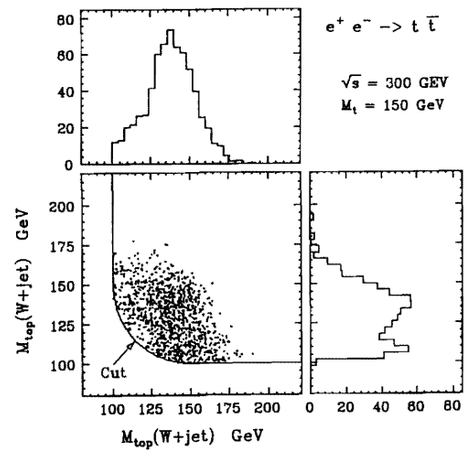

Fig.14 A similar plot for the invariant masses of the 3-jet systems reconstructed as bW candidates at the $t\bar{t}$ threshold.

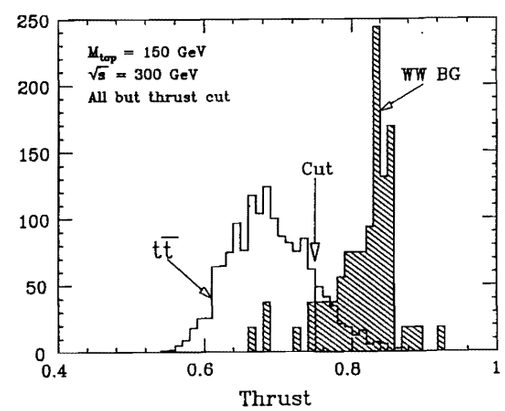

Fig.15 Thrust distributions for the $t\bar{t}$ signal and the W^+W^- background with all but the thrust cut indicated by an arrow.

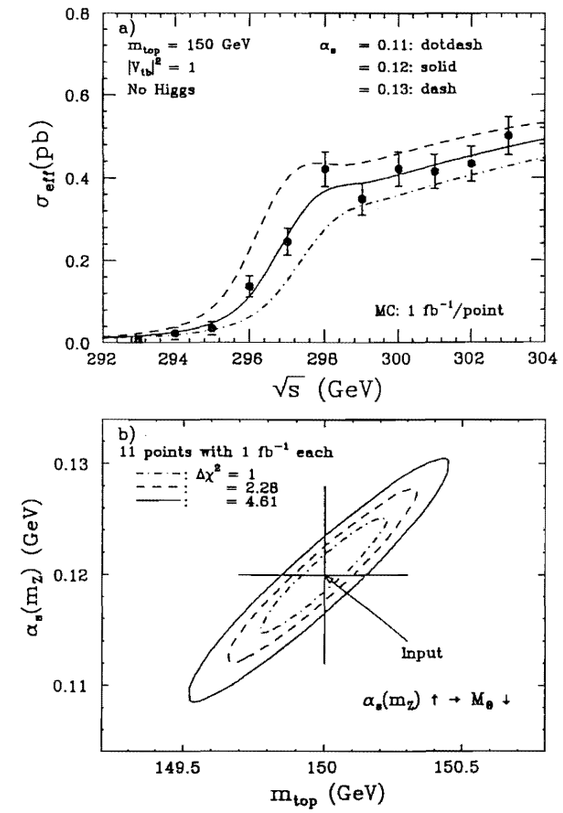

Fig.16 (a) An example of energy scan to determine m_t and $\alpha_s(M_Z)$ where each point corresponds to 1 fb^{-1}. (b) The contour resulting from the fit to the data points.

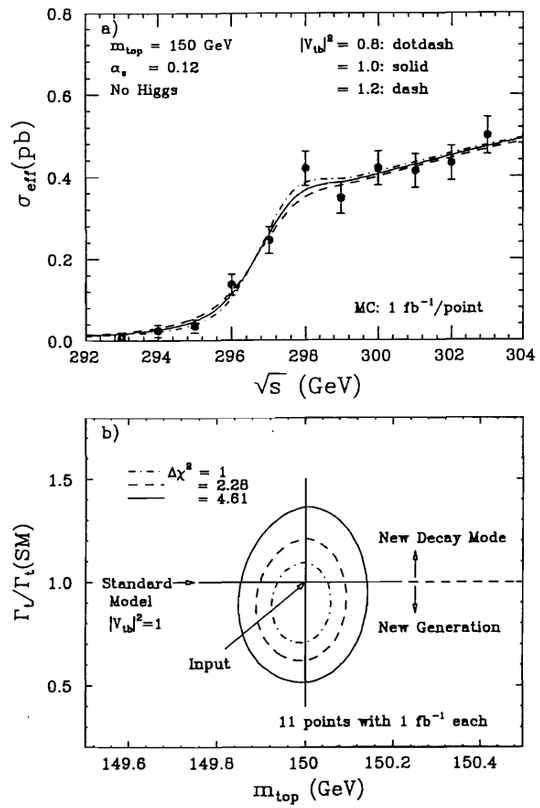

Fig.17 (a) An example of energy scan to determine m_t and $|V_{tb}|^2$ where each point corresponds to 1 fb^{-1}. (b) The contour resulting from the fit to the data points.

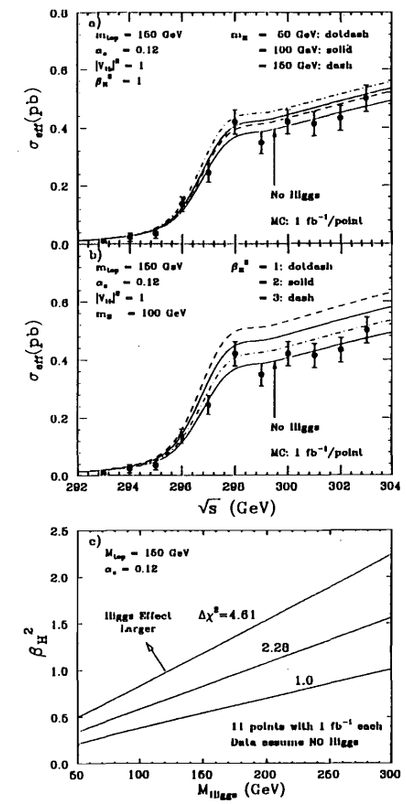

Fig.18 (a) An example of energy scan to determine M_H and β_H^2 where the effective cross section curves are superimposed for several M_H values. (b) The same plot with the effective cross section curves for several β_H^2 values. (c) The contour resulting from the fit to the data points.

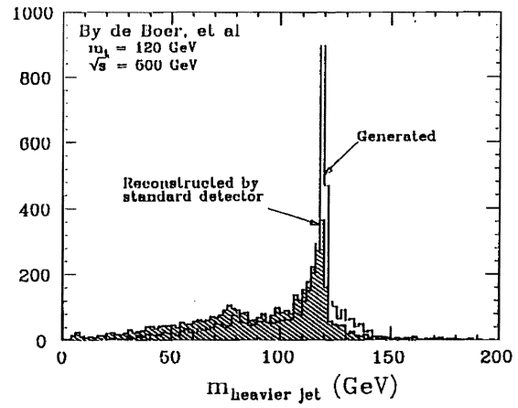

Fig.19 Heavier hemispher mass distributions for m_t = 120 GeV and $\sqrt{s}$ = 500 GeV. The open histogram is the distribution of generated events while the hatched histogram is that of reconstructed events.

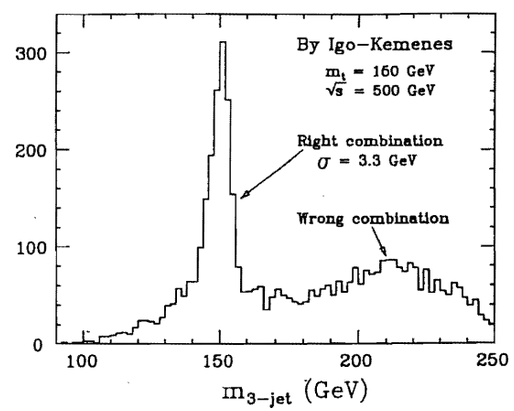

Fig.20 Invariant mass distribution for the 3-jet system resulting from $t \to bW$ decays.

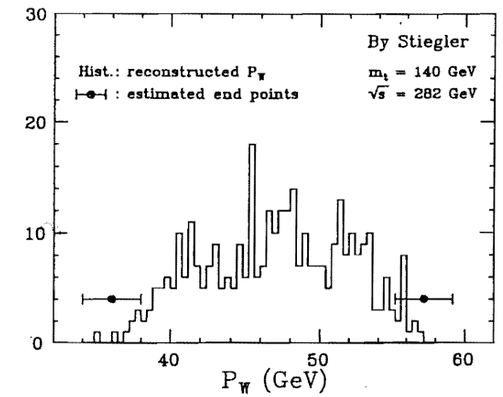

Fig.21 The momentum distribution of Ws from t decays for m_t = 120 GeV and $\sqrt{s}$ = 282 GeV.

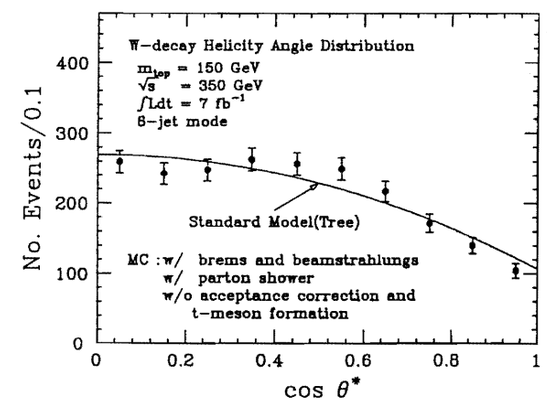

Fig.22 Helicity angle of q or $\bar{q}$ from W decay.

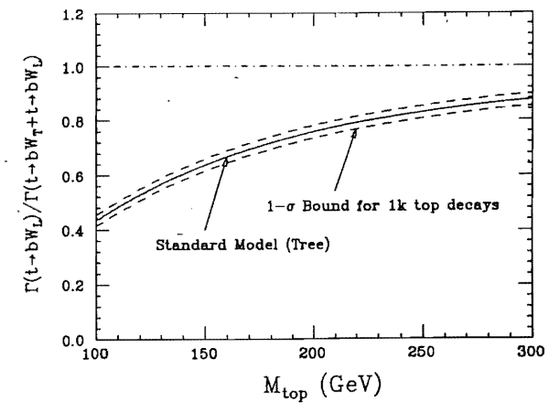

Fig.23 Branching fraction of the $t \to bW_L$ decay as a function of m_t. The dashed curves indicate 1-σ boundaries expected for 1k top decays.

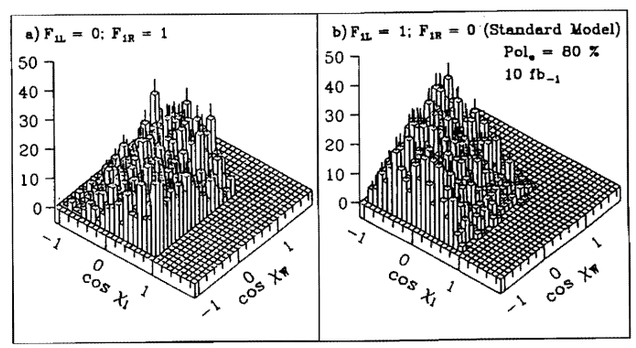

Fig.24 The top decay angle distributions for (a) $F_{1L} = 0$ and $F_{1R} = 1$ and (b) $F_{1L} = 1$ and $F_{1R} = 0$(Standard Model). χ_W is the helicity angle of W in the t rest frame and χ_l is the helicity angle of the lepton in the W rest frame.

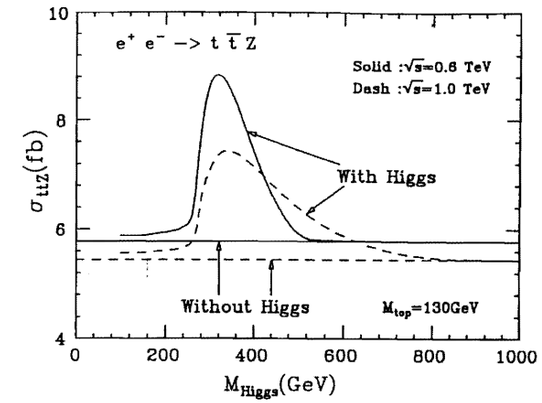

Fig.25 The cross sections for $e^+e^- \to t\bar{t}Z$ at $\sqrt{s} = 0.6$(solid line) and 1.0 TeV(dashed line) for $m_t = 130$ GeV as functions of Higgs mass. For comparison, the cross sections for no Higgs case are also shown.

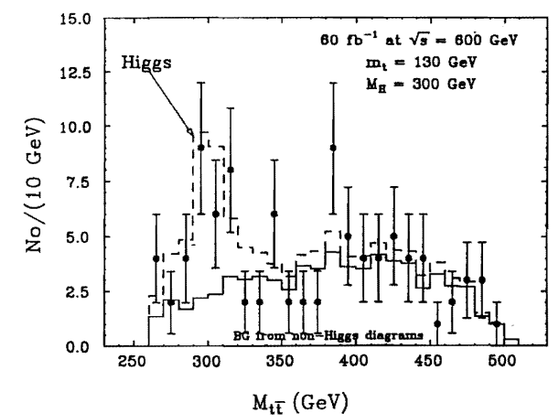

Fig.26 The invariant mass of the $t\bar{t}$ system for the process $e^+e^- \to t\bar{t}Z$, where $m_t = 130$ GeV, $M_H = 300$ GeV, and $\sqrt{s} = 0.6$ TeV. Data points are Monte Carlo result corresponding to 60 fb^{-1}. The solid histogram is the background from non-Higgs diagrams, while the dashed includes the contribution from Higgs decays.

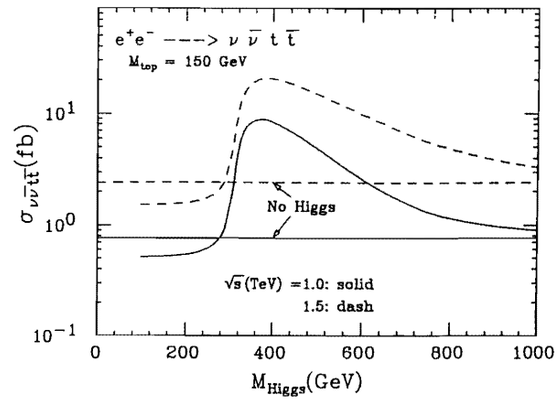

Fig.27 The cross sections for $e^+e^- \to \nu\bar{\nu}t\bar{t}$ at $\sqrt{s} = 1.0$(solid line) and 1.5 TeV(dashed line) for $m_t = 150$ GeV as functions of Higgs mass. The cross sections for no Higgs case are also plotted to see the virtual Higgs contribution.

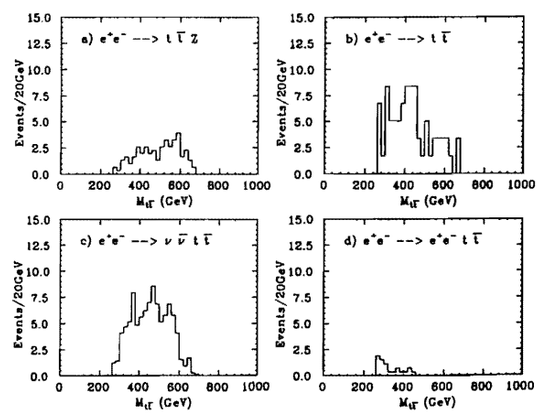

Fig.28 The invariant mass distributions for the $t\bar{t}$ system for (a) $e^+e^- \to t\bar{t}Z$, (b) $e^+e^- \to t\bar{t}$, (c) $e^+e^- \to \nu\bar{\nu}t\bar{t}$, and (d) $e^+e^- \to e^+e^-t\bar{t}$, where $m_t = 150$ GeV, $M_H = 600$ GeV, and $\sqrt{s} = 1.0$ TeV are assumed. The number of events corresponds to an integrated luminosity of 300 fb^{-1}.